YALE
PEABODY
MUSEUM

P.O. BOX 208118 | NEW HAVEN CT 06520-8118 USA | PEABODY.YALE. EDU

JOURNAL OF MARINE RESEARCH

The *Journal of Marine Research,* one of the oldest journals in American marine science, published important peer-reviewed original research on a broad array of topics in physical, biological, and chemical oceanography vital to the academic oceanographic community in the long and rich tradition of the Sears Foundation for Marine Research at Yale University.

An archive of all issues from 1937 to 2021 (Volume 1–79) are available through EliScholar, a digital platform for scholarly publishing provided by Yale University Library at https://elischolar.library.yale.edu/.

Requests for permission to clear rights for use of this content should be directed to the authors, their estates, or other representatives. The *Journal of Marine Research* has no contact information beyond the affiliations listed in the published articles. We ask that you provide attribution to the *Journal of Marine Research*.

Yale University provides access to these materials for educational and research purposes only. Copyright or other proprietary rights to content contained in this document may be held by individuals or entities other than, or in addition to, Yale University. You are solely responsible for determining the ownership of the copyright, and for obtaining permission for your intended use. Yale University makes no warranty that your distribution, reproduction, or other use of these materials will not infringe the rights of third parties.

This work is licensed under a Creative Commons Attribution-NonCommercial-ShareAlike 4.0 International License.
https://creativecommons.org/licenses/by-nc-sa/4.0/

Journal of Marine Research, 49, 619–633, 1991

Journal of MARINE RESEARCH

Volume 49, Number 4

Generation and propagation of inertial waves in the subtropical front

by Dong-Ping Wang[1]

ABSTRACT

A primitive-equation numerical model is used to examine the generation and propagation of internal-inertial waves in the Subtropical Front. The mesoscale variability in surface inertial currents is induced by radiation of internal-inertial waves out of the surface layer. On the warm side of the front, surface inertial energy is carried away by normal internal-inertial waves. A deep inertial energy maximum exists at the base of the thermocline where the effective local inertial frequency approaches the planetary inertial frequency. On the cold side of the front, the surface inertial energy is carried away by anomalously low frequency internal waves. A subsurface inertial energy maximum occurs at the top of the thermocline where the density slope becomes flat. The propagation of internal-inertial waves is consistent with the WKB approximation. On the other hand, since the upper-ocean response consists of a full spectrum of internal-inertial waves, prediction of inertial energy distribution based on ray theory is invalid. Comparison between model results and current profiler observations in the Subtropical Front is quite favorable.

1. Introduction

Inertial (near-inertial) motions in the upper ocean are mainly generated by the wind. Theory for the wind generation of inertial motion correlates the horizontal scale of the inertial wave to the scale of the wind field. Since the horizontal scales of atmospheric forcing usually are very large, inertial motions in the upper ocean are expected to have coherence lengths of over hundreds to thousands of kilometers (Pollard, 1980; Chereskin, *et al.,* 1989). One-dimensional models which form the

1. Marine Sciences Research Center, State University of New York, Stony Brook, New York, 11794, U.S.A.

basis for mixed-layer dynamics, are built upon the rationale that inertial motions are large-scale and are almost completely confined to the mixed layer. On the other hand, observations indicate that surface inertial energy frequently escapes below the mixed layer. In fact, about half of the total energy in internal waves is in the near-inertial band (D'Asaro, 1985; Gregg, *et al.,* 1986).

According to internal wave theory, if surface inertial motion has large horizontal length scale, its vertical group velocity must be very small. Thus, presence of energetic inertial waves in the thermocline suggests a strong mesoscale variability in surface inertial currents. The mesoscale variation in surface inertial currents can be generated at the wake of a traveling storm (Price, 1983). D'Asaro (1985) showed evidence for the downward penetration of storm-generated inertial waves. The mesoscale surface variability also can be generated by small-scale variations in the wind field (Gill, 1984). Paduan and DeSzocke (1989) showed evidence for such mesoscale inertial current variations. In addition, the mesoscale variability can be induced by the planetary β effect which acts as a large-scale vorticity gradient (D'Asaro, 1989).

In the upper ocean, mesoscale eddy and frontal activities are common. Interaction between these mesoscale oceanic features and the initially large-scale wind-generated inertial wave field may lead to the subsequent mesoscale variability in surface inertial currents. According to Kunze (1985), inertial energy originated in the warm side of a surface front will propagate downward and is trapped at the critical layer. Observations indeed indicate enhanced subsurface inertial energy in the front, particularly, on the warm (anticyclonic) side (Kunze and Sanford, 1984; Kunze, 1985; Mied *et al.,* 1986; Weller, 1985). However, Kunze (1985) only studied the problem of propagation of internal-inertial wave in a front. A general treatment of the upper-ocean response to wind forcing should include both generation and propagation of inertial energy in a frontal zone. In this paper a primitive-equation numerical model is used to study the two-dimensional (assuming no variation in the along-front direction) problem of generation and propagation of inertial motion in a front. The model suggests that the mesoscale oceanic front and eddy is effective in channeling the surface inertial energy into the thermocline.

2. Model

The numerical model used in this study is the two-dimensional version of a primitive-equation, coastal ocean circulation model (Wang, 1985; 1990). The two-dimensional assumption is common in theoretical studies (e.g., Mooers, 1975; Kunze and Sanford, 1984), as the cross-frontal scale typically is much smaller than the along-frontal scale. However, the two-dimensional assumption eliminates the Doppler effect. The numerical model is hydrostatic and is fully nonlinear in the momentum and buoyancy equations. For comparison, internal wave theory usually includes vertical acceleration (nonhydrostatic), but neglects nonlinear terms (for

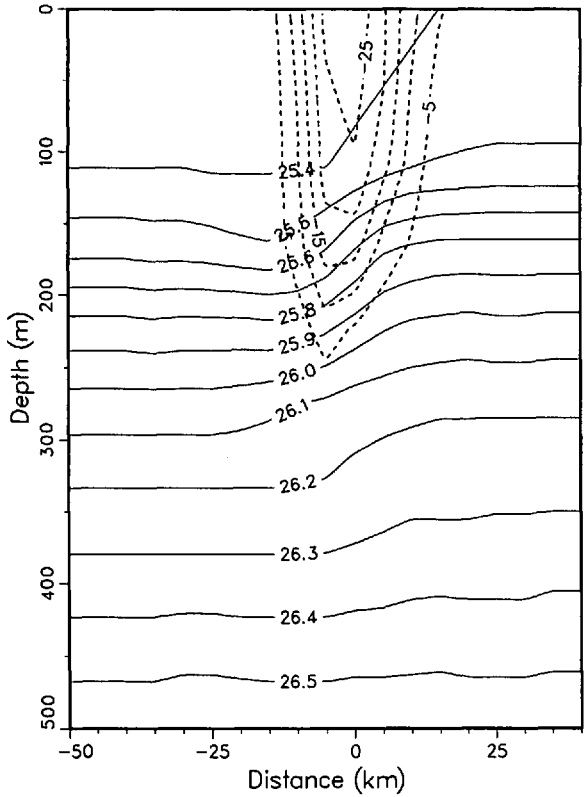

Figure 1. The cross-frontal distribution of density (σ_t) and along-front velocity (cm s^{-1}).

example, Section 8.4, Gill, 1982). Since the inertial frequency is much lower than the buoyancy frequency, use of the hydrostatic assumption in this study is well justified. Inclusion of the nonlinear buoyancy advection allows consideration of the horizontal density gradient. In the frontal zone, the horizontal density advection is comparable to the vertical density advection. Hence, retaining the full density advection equation is essential. Inclusion of the nonlinear momentum term allows wave—mean current interaction; although the effect is minimal in this study. The model also includes a one-dimensional turbulence closure submodel for calculation of eddy viscosities in the mixed layer (Chen and Wang, 1990).

The model domain is a two-dimensional (in x-z plane) channel, 1000 m deep and 400 km wide. The horizontal resolution is 5 km, and the vertical resolution is 50 m in the upper 500 m and 100–200 m in the lower water column. Resolution sensitivity test by doubling the number of vertical grids shows no quantitative difference. The constant horizontal eddy diffusivity is 10^5 cm^2 s^{-1}. The vertical eddy diffusivity below the mixed layer is derived from the Munk-Anderson formula; the coefficients corresponding to the neutral condition are 0.1 cm^2 s^{-1} for temperature and 1 cm^2 s^{-1}

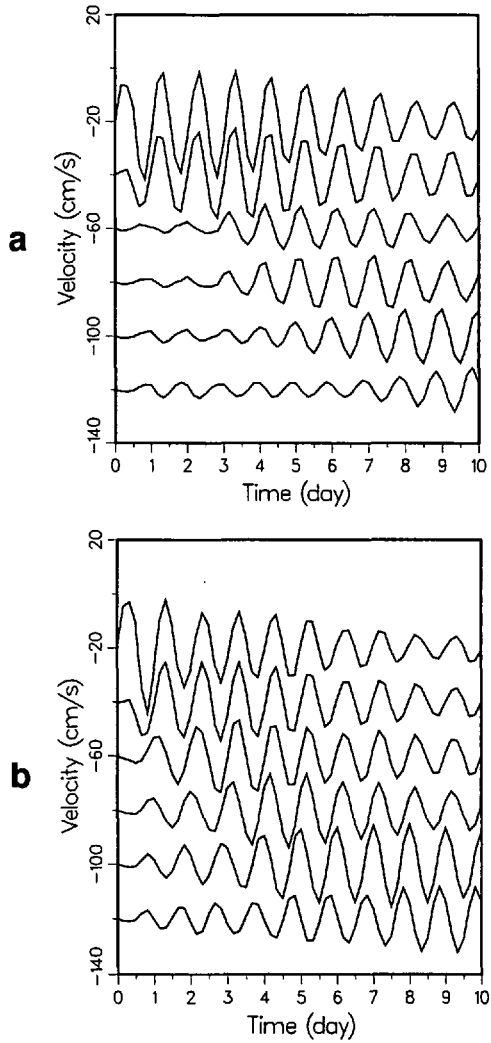

Figure 2. The cross-frontal velocity profiles (cm s^{-1}) at upper 6 vertical levels (in 50 m increment) starting from the beginning of wind forcing: (a) $x = -20$ km, (b) $x = -10$ km, and (c) $x = 10$ km. (The velocity axis is shifted by 20 cm s^{-1} in each level.)

for momentum. The actual vertical eddy viscosity in the stratified water column is typically < 0.1 $cm^2 s^{-1}$. The boundary conditions are zero normal flow at the sidewall, quadratic friction at the bottom, and free surface.

The initial density distribution is a geostrophic front derived from the density observation in the Subtropical Front (Roden, 1981). Figure 1 shows the initial density and geostrophic current distribution; the density profile only changes slightly during the 10-day simulation. The front is 30 km wide and 300 m deep. The geostrophically balanced current has a maximum speed of about 30 cm/s, located at

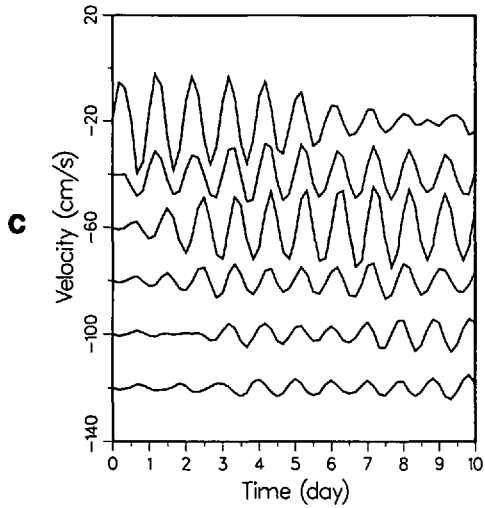

Figure 2. (Continued)

the center of the channel (200 km from the wall, or, $x = 0$ km in Fig. 1). At 30N, the local inertial period is 1 day. The mean horizontal shears are about $\pm 0.3 f$ (f is the Coriolis parameter). The external forcing is a spatially uniform, cross-channel wind. Sensitivity test indicates that model results are not affected by the direction of wind forcing. A 20 m/s wind burst of 12 hr duration (half inertial period) is abruptly imposed. The choice of wind forcing is to maximize the partition of wind-generated energy into the inertial motion (Veronis, 1956). This approach is in contrast to typical circulation model studies which gradually (over several inertial periods) turn on the wind to avoid excitation of the inertial motion.

3. Base case

The model is initialized by running without wind forcing for 1 day, in order to confirm that no inertial current is generated by the imposed geostrophic current. Then, the wind pulse is turned on, and the model is run for an additional 10 days. Immediately after the wind is applied, vigorous wind-generated turbulence extends through the initially imposed mixed layer (of 100 m depth). The inertial current in the mixed layer is about 30 cm/s, and is uniform everywhere except very near the coast where the inertial motion is inhibited by the coastal wall. After the wind is turned off, surface inertial currents within the front experience very complicated adjustment processes. Figure 2a–2c shows the cross-frontal velocity profiles at $x = -20$ km (outside the front), $x = -10$ km (warm side of the front) and $x = 10$ km (cold side of the front) for the top 500 m from day 0 (the start of wind forcing) to day 10. In all figures, the x-coordinate is referenced to Figure 1.

Off the warm side of the front, the inertial energy stays in the mixed layer (Fig. 2a). The flow adjustment is consistent with the one-dimensional assumption that the inertial energy is trapped and remains almost constant in the mixed layer. (Since the plots are based on 4-hourly re-sampled model outputs, the peak amplitudes sometimes appear to be truncated.) However, the one-dimensional result eventually breaks down. For example, after day 5, significant inertial oscillations appear in the mid-depths well below the mixed layer. In other words, the two-dimensional effect can extend beyond the physical boundary of the front. Off the cold side of the front (not shown), the flow adjustment is similar to that off the warm side of the front, except that the deep inertial oscillation is weaker. The propagation of inertial energy out of the frontal zone will be discussed later.

On the warm side of the front ($x = -10$ km), the inertial energy in the mixed layer quickly propagates into the thermocline (Fig. 2b). In 5 days (or, 5 inertial cycles), most of the surface inertial energy in the warm frontal zone has disappeared, and the largest inertial oscillation is at the thermocline. The wave packet propagates downward, but the phase propagation for each individual wave is upward. In other words, the group velocity is opposite to the phase velocity, which is consistent with the property of normal internal-inertial waves. On the cold side of the front, the inertial energy at the surface also rapidly moves downward (Fig. 2c). However, unlike that in the warm side, most of the subsurface inertial energy is retained in the upper 150 m above the thermocline. Also, the phase propagation is downward. As both the group velocity and the phase velocity are downward, the internal-inertial wave in the warm side has *anomalous* behavior. The striking contrast of flow adjustment between the warm and the cold sides of the front highlights the interaction between internal-inertial waves and the mean flow. It is also noted that on the cold side of the front a strong vertical shear exists in the mixed layer after day 5 (Fig. 2c). In contrast, the mixed layer structure is normal in the warm side of the front (Fig. 2b).

The kinetic energy of internal-inertial waves is defined as $\langle (u - \langle u \rangle)^2 + (v - \langle v \rangle)^2 \rangle / 2$, where $\langle \ldots \rangle$ is average over one inertial period (1 day). Through the 10-day simulation, the mean along-frontal jet changes gradually, and the mean cross-frontal velocity remains essentially zero. Figure 3a and 3b shows the wave kinetic energy distribution (in log 10 base) at the warm ($x = -10$ km) and the cold ($x = 10$ km) sides of the front. On the warm side, the energy maximum quickly descends to the thermocline with a vertical group velocity Cg_z of about 30 m day^{-1} in the first 5 days (Fig. 3a). The wave packet is coherent from surface to thermocline with a vertical wavelength λ_z of about 300 m. The internal-inertial waves stay in the thermocline in the second 5 days, and the much smaller vertical group speed Cg_z is about 10 m day^{-1}. The wave energy becomes concentrated in the thermocline with a vertical wavelength λ_z of about 100 m. In contrast, on the cold side of the front, the wave energy remains trapped in the upper water column for the entire 10 day period (Fig. 3b). Also, despite the rapid depletion of surface inertial energy, the energy never

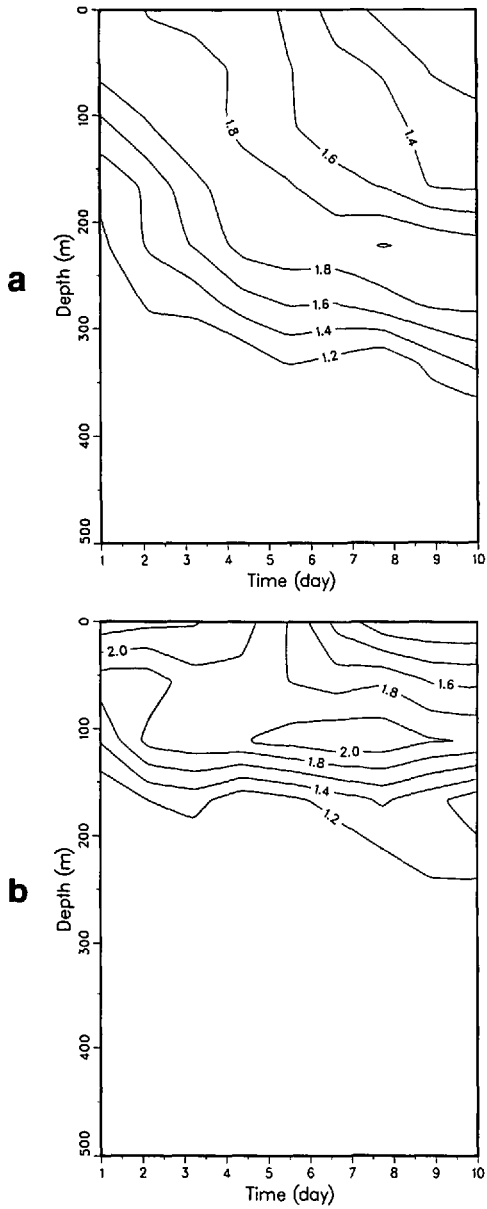

Figure 3. The averaged wave kinetic energy distribution (in log 10 base, with unit = $cm^2\ s^{-2}$) for the base case: (a) $x = -10$ km (warm side), and (b) $x = 10$ km (cold side).

penetrates further downward. This suggests that the surface inertial energy on the cold side of the front spreads away laterally.

Figure 4a and 4b shows the wave kinetic energy distribution across the front at day 4 and day 9. Downward penetration of the surface inertial energy is almost entirely

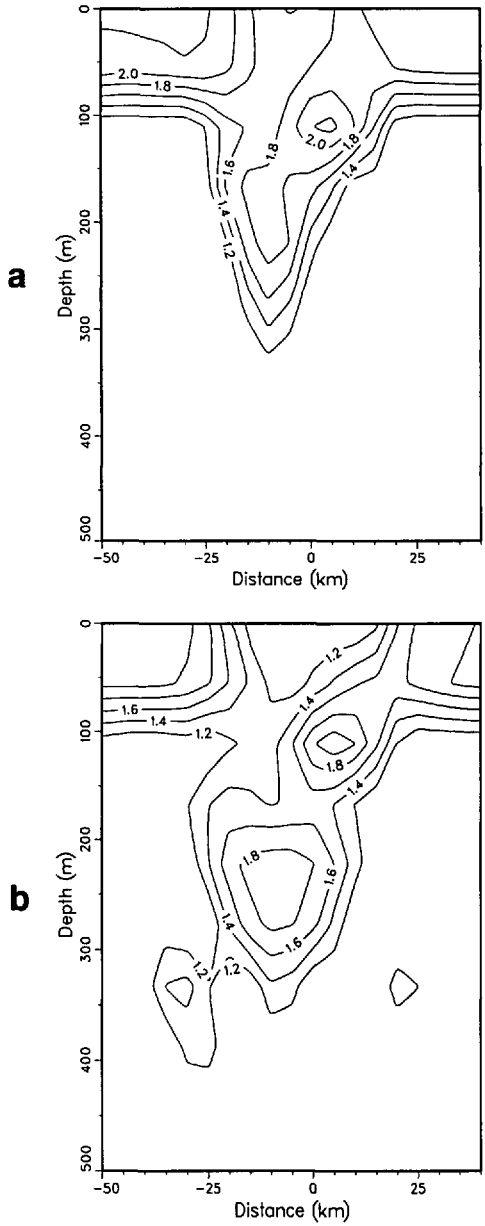

Figure 4. The averaged wave kinetic energy distribution (in log 10 base, with unit = $cm^2 s^{-2}$) for the base case: (a) day 4, and (b) day 9.

confined to the front, indicating that the horizontal wavelength is about the width of the front. At day 4, the inertial energy on the warm side is uniform in the upper 200 m, whereas the inertial energy on the cold side is concentrated at around 120 m. By day 9, the deep inertial energy on the warm side of the front forms a well defined

core centered around 250 m. On the other hand, the energy maximum on the cold side remains unchanged. The location of the energy maximum rises abruptly from the warm side to the cold side. It is also noted that the deep inertial energy extends well beyond the physical boundary of the front.

4. Comparison with ray theory

The normal propagation of internal-inertial waves occurs in the region where the wave frequency is higher than the effective local inertial frequency f_{eff} (Mooers, 1975),

$$f_{eff}^2 = \left(f + \frac{\partial V}{\partial x}\right) f. \tag{1}$$

The maximum horizontal vorticity in the frontal zone is about $\pm 0.3\, f$. Thus, for incident waves of planetary inertial frequency f, free waves can exist only on the negative vorticity (warm) side of the front.

Kunze and Sanford (1984) and Kunze (1985) studied the internal-inertial wave propagation through a front using ray theory. A basic assumption in ray theory is that the fundamental wave dispersion relation is locally valid. For internal-inertial waves, the vertical group velocity is related to the aspect ratio $S_x = \lambda_z/\lambda_x$, the ratio between vertical and horizontal wavelengths, and the buoyancy frequency squared N^2, by (Section 8.4 of Gill, 1982)

$$Cg_z \approx \frac{N^2 \lambda_z S_x^2}{2\pi f}. \tag{2}$$

Model results indicate that during the first 5 days, the internal-inertial waves on the warm side of the front are in the upper 250 m. Using $N^2 \approx 0.8 \times 10^{-5}\ \mathrm{s}^{-2}$, $Cg_z =$ 30 m/day, and $\lambda_z = 300$ m, the horizontal wavelength λ_x calculated from Eq. 1 is 35 km, which is about the width of the front. In other words, the local dispersion relation is satisfied. For the second 5 days, the internal-inertial waves are in the thermocline. The local dispersion relation again is satisfied, as the increase in stratification ($N^2 \approx 5 \times 10^{-5}\ \mathrm{s}^{-2}$) is compensated by the decrease in vertical group velocity ($Cg_z = 10$ m/day) and vertical wavelength ($\lambda_z = 100$ m). Thus, despite the sharp variation in density stratification, the WKB approximation is valid.

In Kunze and Sanford (1984), near-inertial waves (where near-inertial is taken to be slightly above the effective local inertial frequency) are assumed to originate from the surface. Waves starting in the negative vorticity trough will have frequencies below the effective local inertial frequency outside this region, so they will not be able to propagate away. As waves in the negative vorticity trough propagate downward, they encounter an increasing effective local inertial frequency. To continue to satisfy the dispersion relation, the vertical wavelength must shrink to zero and the wave will stall; the singularity occurs at the critical layer where the wave frequency equals the

effective local inertial frequency. Kunze and Sanford (1984) suggests that critical layer absorption is a major sink for the downward energy flux. Model results indicate trapping of inertial energy in the warm side (negative vorticity trough). The sudden stall of downward energy propagation at day 5 is clearly related to the fact that $f_{eff} \rightarrow f$ at the base of the thermocline. On the other hand, model results indicate outward spreading of the deep inertial energy beyond the front, which contradicts the prediction by ray theory.

In the ray tracing approach, only a single wave of constant frequency is considered. The underlying assumption is that the final solution can be described by a linear superposition of single-wave solutions. However, because internal-inertial waves are strongly dispersive, the final solution may not be readily inferred from single-wave solution. This type of response is best illustrated in the classical transient Rossby adjustment problem (Section 7.3, Gill, 1982). Since the dispersion of an initial pressure jump involves radiation of a spectrum of Poincare waves, the wave frequency at a fixed point is not constant, but, it tends to decrease with time toward the inertial frequency (for which the group velocity is minimum). A similar behavior is found in model results that dominant frequencies tend to f with time. In the first 5 days, wave frequencies are less than f on the warm side, but higher than f on the cold side. (The wave *frequency* is determined by simply following the revolution of phase angle, $\tan^{-1} u/v$.) However, wave frequencies are close to f on both sides in the second 5 days.

According to Kunze and Sanford (1984), waves starting in the positive vorticity ridge will have frequencies above the effective local inertial frequency outside this region, so are free to propagate out. Hence, no internal-inertial wave can be trapped in the cold side of the front. The model, however, indicates energetic near-inertial oscillations trapped between the mixed layer and the thermocline. Furthermore, the downward transfer of surface inertial energy is associated with downward phase propagation. This anomalous feature is caused by the interaction between internal-inertial wave and sloping density front. According to Mooers (1975), free internal-inertial waves can exist at anomalously low frequencies: $\sigma_l < \sigma < f_{eff}$

$$\sigma_l^2 = f_{eff}^2 - s^2 N^2. \tag{3}$$

The slope of isopycnals $s = -M^2/N^2$, where M^2 is the horizontal density gradient. The sloping isopycnal will modify the effective local inertial frequency when the vertical shear is large (via the thermal wind relation) and the density stratification is weak. It is obvious from Figure 1 that a steep isopycnal slope exists in the upper 100 m on the cold side of the front. Above the thermocline (upper 150 m), the effective local inertial frequency f_{eff} is $\sim 1.13 f$, and the frequency modification due to the sloping isopycnal is $\sim 0.05\ f$. Thus internal-inertial waves with frequencies between $1.08\ f$ and $1.13\ f$ can be trapped in the upper water column. The model

shows that the wave frequency in the cold side of the front is about 1.1 f. Anomalously low frequency waves are stalled at the top of the thermocline where $\sigma_l \rightarrow f_{eff}$.

A peculiar property of the anomalously low frequency wave is that the phase propagation is downward for downgoing waves; the term *downgoing* indicates the direction of energy propagation (group velocity). The characteristic for downgoing wave (Mooers, 1975) is

$$\left(\frac{\lambda_z}{\lambda_x}\right) = -s + \left(s^2 + \frac{\sigma^2 - f_{eff}^2}{N^2}\right)^{1/2}. \tag{4}$$

For $\lambda_x > 0$, under the normal condition of no isopycnal slope, $s = 0$, the downgoing wave propagates upward (that is, $\lambda_z > 0$). However, in the anomalously low frequency band, the downgoing wave propagates downward ($\lambda_z < 0$), as the second term on the RHS of Eq. 3 is less than s. The fact that model also shows a downward phase propagation is strong evidence for the presence of anomalously low frequency waves on the cold side of the front. It should be noted that trapping of the anomalously low frequency wave occurs only in the vertical. Waves are free to propagate horizontally towards the warm side where $f_{eff} < f$. Channeling of inertial energy from the upper water column of the cold side into the interior of the warm side is indicated in the energy distribution (Fig. 4a–4b).

5. Comparison with observations

Kunze and Sanford (1984) found strong inertial waves in the Subtropical Front. Our model study uses the same density data, so model results can be directly compared with observations. The most striking feature in the observations was the strong intensification of clockwise inertial energy on the warm edge of the front. This intensification was in the form of a sharp peak, rising by a factor of 4 above the background level of 1.6 J m^{-3} and having a half-energy width of 10 km. The energy peak did not change position or intensity between two profiles taken 4 days apart, suggesting a persistent feature. Our model shows sharply peaked internal wave energy in the thermocline (Fig. 4b). The energy peak is located at $x = 10$ km on the warm edge (see Fig. 1 for the density structure across the front). The background energy level is 1.6 J m^{-3} (1.2 in log 10 base, Fig. 4b), the maximum energy is a factor of 4 higher (1.8 in log 10 base), and the half energy width is 12 km. The perfect agreement is probably coincidental, which nevertheless substantiates the claim that the observed intense deep inertial energy peak is originated from directly above.

Kunze and Sanford (1984) made a rough estimate of the internal-inertial wave characteristics from the velocity profilers taken across the front. Given the uncertainties associated with the limited number of observations, the energetic downward-propagating waves had horizontal wavelength $\lambda_x = 20 \pm 13$ km, vertical wavelength $\lambda_z = 120 \pm 30$ m, and $Cg_z = 19 \pm 17$ m day^{-1}. Model results are $\lambda_x = 31$ km, $\lambda_z = 100$ m, and $Cg_z = 10$ m day^{-1}, which agree well with their estimate. Unfortunately,

since data were not reliable in the upper 100 m, the prediction of a sharp variation of surface inertial energy across the front cannot be verified. The anomalously low frequency waves on the positive vorticity ridge also cannot be tested. However, observations showed a sudden rise of locations of the energy maxima from the warm side to the cold side, which may be indicative of the energetic anomalously low frequency waves.

6. Sensitivity study

The model domain ideally should be unbounded. Under such a configuration, no internal wave energy source exists outside the front for a spatially uniform wind forcing. In the present setup of a 400 km wide channel, internal waves are excited at the coast. The generation of internal-inertial waves at the coast, which has been considered by Millot and Crepon (1981) and Kundu *et al.* (1983), is examined in a separate study (Tintore *et al.,* 1991). The internal-inertial waves generated within the coastal zone ($\sim$45 km) will influence the entire channel. However, the background noise is rather small. A model run without a density front indicates that the background energy level in the central part of the channel never exceeds 1.2 (log 10 base).

The model run is repeated by reducing the density contrast across the front to half of the base value. Figure 5a and 5b shows the energy distribution across the front at day 4 and day 9. On the warm side of the front, the downward energy penetration is less than in the base case; however, the energy distribution is similar. On the other hand, on the cold side of the front, the energy trapping in the upper water column is barely noticeable. To have significant contribution from anomalously low frequency waves, the isopycnal slope must be strong. For a weak density front, that contribution becomes negligible. The extraction of surface inertial energy, nevertheless, is still quite effective in a weak front. At day 9, the surface inertial energy in the warm side of the front is about 25% of the ambient surface energy, but, relatively higher surface energy remains in the cold side.

7. Discussion

This study examines two fundamental aspects of the near-inertial motion, namely, the wind-generation of surface inertial currents in a front and the propagation of inertial-internal waves through a front. Due to the variation of effective local inertial frequency across the front, a large-scale wind forcing will generate a flow divergence with length scales comparable to the mesoscale frontal width. Klein and Hua (1988) examined the heterogeneity of a surface mixed layer in the mesoscale flow field using a quasigeostrophic model. They clearly demonstrated the effect of geostrophic front on wind-generated inertial currents (and mixed layers). However, in a quasigeostrophic model, the surface inertial energy is removed only through frictional

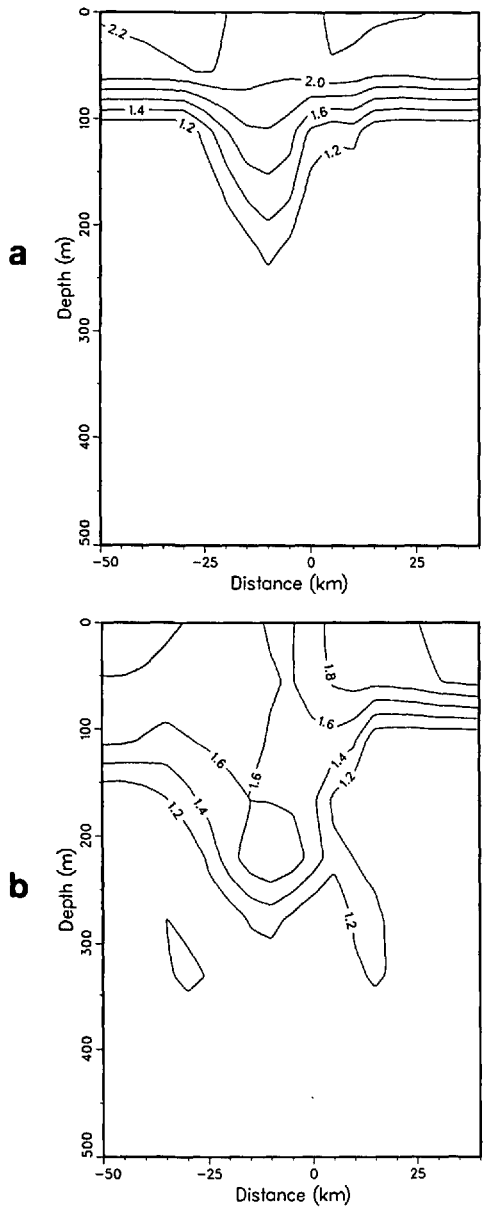

Figure 5. The averaged wave kinetic energy distribution (in log 10 base, with unit = $cm^2\ s^{-2}$) for the weak-front case: (a) day 4, and (b) day 9.

dissipation. The present study using a primitive-equation model indicates that internal-inertial waves are much more effective in removing the surface inertial energy from the frontal zone. Thus, strong mesoscale variabilities in surface inertial energy and mixed-layer depth are expected to result from the interaction between

large-scale wind forcing and the mesoscale front. Recent observations (Weller *et al.*, 1991) confirm that inertial variabilities in the subtropical convergence zone have length scales much smaller than the horizontal scales of wind stress.

Ray theory is useful in describing the propagation of internal-inertial waves in an ambient vorticity field. The model shows that the WKB approximation is valid even when the vertical wavelength is comparable to the vertical extent of the front. Thus, in the warm side of the front, as internal-inertial waves propagate into the thermocline, the energy peak will shift from low wavenumber ($\lambda_z \sim 300$ m) to high wavenumber ($\lambda_z \sim 100$ m). On the other hand, use of ray theory in analysis of the upper ocean response is inappropriate. Relaxation of the forced surface inertial motion excites a full spectrum of internal-inertial waves. Waves with frequencies higher than f are free to propagate through the warm side of the front unimpeded. Only waves with frequencies between f and f_{eff} are trapped, but they carry only a fraction of the total energy flux. In other words, the deep inertial waves in the warm side of the front are not the consequence of focusing of *all* surface energy flux, as implied in ray theory. Rather, they are the remanent of internal-inertial waves whose frequencies are very close to f. Trapping of inertial energy in the thermocline can lead to vigorous interior mixing. Lueck and Osborn (1986) showed a striking example of enhanced vertical mixing at the base of a warm core ring.

The *discovery* of anomalously low frequency internal-inertial waves in the cold side of the front is unanticipated. Although a passband below the effective local inertial frequency is theoretically plausible (Mooers, 1975), this study is the first to demonstrate that such waves do exist. More importantly, the anomalously low frequency waves play a central role in carrying the surface inertial energy away from the positive vorticity ridge. The existence of anomalously low frequency wave needs to be verified. The effect of sloping density surface also needs to be included in the study of wave—front interaction.

Acknowledgments. This study was supported by the National Science Foundation. The model computing was done at the Cornell National Supercomputer Facilities which is sponsored by the National Science Foundation and IBM. Valuable comments by Eric Kunze on the original manuscript motivated re-examination of model results. This paper owes greatly to his generous effort as a reviewer. I also appreciate the comments by Hartmut Peters and an anonymous reviewer.

REFERENCES

Chen, D. and D.-P. Wang. 1990. Simulating the time-variable coastal upwelling during CODE 2. J. Mar. Res., *48,* 335–358.

Chereskin, T. K., M. D. Levin, A. J. Harding and L. A. Regier. 1989. Observations of near-inertial waves in acoustic doppler current profiler measurements made during the Mixed Layer Dynamics Experiment. J. Geophys. Res., *94,* 8135–8145.

D'Asaro, E. A. 1985. The energy flux from the wind to near-inertial motions in the surface mixed layer. J. Phys. Oceanogr., *15,* 1043–1059.

—— 1989. The decay of wind-forced mixed layer inertial oscillations due to β effect. J. Geophys. Res., *94,* 2045–2056.

Gill, A. E. 1982. Atmosphere-Ocean Dynamics, Academic Press, NY, 662 pp.

—— 1984. On the behavior of internal waves in the wakes of a storm. J. Phys. Oceanogr., *14,* 1129–1151.

Gregg, M. C., E. A. D'Asaro, T. J. Shay and N. Larson. 1986. Observations of persistent mixing and near-inertial waves. J. Phys. Oceanogr., *16,* 856–885.

Klein, P. and B. L. Hua. 1988. Mesoscale heterogeneity of the wind-driven mixed layer: Influence of a quasigeostrophic flow. J. Mar. Res., *46,* 495–525.

Kundu, P. K., Chao, S.-Y. and J. P. McCreary. 1983. Transient coastal currents and inertio-gravity waves. Deep Sea Res., *30,* 1059–1082.

Kunze, E. 1985. Near-inertial wave propagation in geostrophic shear. J. Phys. Oceanogr., *15,* 544–565.

Kunze, E. and T. B. Sanford. 1984. Observations of near-inertial waves in a front. J. Phys. Oceanogr., *14,* 566–581.

Lueck, R. and T. Osborn. 1986. The dissipation of kinetic energy in a warm-core ring. J. Geophys. Res., *91,* 803–818.

Mied, R. P., C. Y. Shen, C. L. Trump and G. J. Lindemann. 1986. Internal-inertial waves in a Sargasso Sea Front. J. Phys. Oceanogr., *16,* 1751–1762.

Millot, C. and M. Crepon. 1981. Inertial oscillations on the continental shelf of the Gulf of Lions: Observations and theory. J. Phys. Oceanogr., *11,* 639–657.

Mooers, C. N. K. 1975. Several effects of a baroclinic current on the cross-stream propagation of inertial-internal waves. Geophys. Fluid Dyn., *6,* 245–275.

Paduan, J. D. and R. A. De Szoeke. 1989. Inertial oscillations in the upper ocean during the Mixed Layer Dynamics Experiment (MILDEX). J. Geophys. Res., *94,* 4835–4842.

Pollard, R. T. 1980. Properties of near-surface inertial oscillations. J. Phys. Oceanogr., *10,* 385–398.

Price, J. F. 1983. Internal wave wake of a moving storm. Part I: Scales, energy budget and observations. J. Phys. Oceanogr., *13,* 949–965.

Roden, G. I. 1981. Mesoscale thermohaline, sound velocity, and baroclinic flow structure of the Pacific Subtropical Front during the winter of 1980. J. Phys. Oceanogr., *11,* 658–675.

Tintore, J., D.-P. Wang and E. Garcia. 1991. Internal-inertial waves in the coastal ocean.

Veronis, G. 1956. Partition of energy between geostrophic and non-geostrophic oceanic motions. Deep-Sea Res., *3,* 157–177.

Wang, D.-P. 1985. Numerical study of gravity currents in a channel. J. Phys. Oceanogr., *15,* 299–305.

—— 1990. Model of mean and tidal flows in the Strait of Gibraltar. Deep-Sea Res., *36,* 1535–1548.

Weller, R. A. 1985. Near-inertial velocity variability at inertial and subinertial frequencies in the vicinity of the California Current. J. Phys. Oceanogr., *15,* 372–385.

Weller, R. A., D. L. Rudnick, C. C. Eriksen, K. L. Polzin, N. S. Oakey, J. W. Toole, R. W. Schmitt, and R. T. Pollard. 1991. Forced ocean response during the Frontal Air-Sea Interaction Experiment. J. Geophys. Res., *96,* 8611–8638.

Received: *30 January, 1991;* revised: *11 July, 1991.*